

0017-9310(95)00162-X

# Computation of turbulent evaporating sprays with well-specified measurements: a sensitivity study on droplet properties

X.-Q. CHEN and J. C. F. PEREIRA†

Instituto Superior Técnico (Technical University of Lisbon), Mechanical Engineering Department,  
Av. Rovisco Pais, 1096 Lisbon Codex, Portugal

(Received 12 October 1994 and in final form 19 April 1995)

**Abstract**—An extensive numerical study was carried out for a confined evaporating spray in a turbulent, heated gas flow using a published well-defined experimental dataset. The Eulerian–Lagrangian stochastic models were employed for spray calculations wherein the gas turbulence was modeled using the second-moment transport model for the Reynolds stresses and heat-flux vectors, and the droplet dispersion was modeled using the Lagrangian stochastic models with or without temporal correlations. Two fashions of the infinite-conduction–evaporation model were studied, both of which have taken into account the variable gas–film properties by the 1/3-rule. Numerical results for the droplet phase, i.e., the mean diameters, mass fluxes, mean and fluctuating velocities were presented and discussed by comparison with the experimental data. The sensitivity of various droplet properties to the number of droplet trajectories at the inlet, the drift correction approaches for the improvement of mass-flux predictions, and the evaporation models was investigated in terms of the well-defined experimental dataset. Results show that the droplet mean velocities are generally not sensitive to all the factors considered, that droplet r.m.s. velocities downstream are sensitive to the number of trajectories, that the droplet mass-flux accumulation near the centreline can be substantially improved by using a new drift correction approach, and that mass-flux predictions are sensitive to the evaporation models.

## INTRODUCTION

Numerical investigation of fuel sprays is a prerequisite for further study of spray combustion. Due to their particular advantage of straightforwardly accounting for droplet trajectory crossings, Lagrangian stochastic separated-flow (SSF) models are increasingly receiving great attention. The comprehensive reviews of spray and combustion models can be found in, among others, Chigier [1], Law [2], Faeth [3], Crowe [4] and Sirignano [5, 6].

Many of early Lagrangian SSF calculations, i.e. Shuen *et al.* [7] and Chen and Pereira [8], have clearly shown that the specification of droplet-phase initial conditions plays an important role in accurate prediction of droplet properties. Without well-specified inlet conditions from the experiment, Sturgess *et al.* [9] found that it is very difficult to yield acceptable predictions of droplet space distribution, even though they spared no effort on adjusting the specification of the assumed inlet conditions. Therefore, accurate assessment of developed Eulerian–Lagrangian SSF models must rely on well-specified experimental data, especially those used as the initial conditions. As a result, recent numerical investigations of sprays were carried out by Bulzan *et al.* [10] and Chang *et al.* [11] under detailed initial conditions. Moreover, systematically experimental and theoretical study has also been

made earlier on nonevaporating sprays in the Faeth's group; see Solomon *et al.* [12, 13]. Their numerical results show that Eulerian–Lagrangian SSF models can achieve encouraging results. However, all these studies were associated with nonevaporating sprays. Currently, few complete sets of experimental measurements are available for evaporating sprays. Aggarwal and Chitre [14] computed a turbulent evaporating spray based on some assumed inlet conditions, with the aim of qualitatively studying the effect of various evaporation models. Even though experimental and numerical study has been made by Solomon *et al.* [15] on evaporating sprays, their numerical results were obtained using the measurements only downstream of 50 nozzle diameters. Recently, Sommerfeld *et al.* [16] have successfully performed experimental measurements of turbulent evaporating sprays, which make it possible to investigate numerical models on the prediction of evaporating sprays. To attain accurate predictions, it is significant to perform a study on the sensitivity of droplet properties, i.e. velocities, diameters and mass fluxes, to such factors as the number of droplet trajectories, Lagrangian SSF models and evaporation models, etc. Therefore, the main objective of this work is to clarify the effect of these factors on droplet properties in terms of available, well-specified, experimental measurements in an attempt to get an insight into the influence of the numerical models on the prediction of spray evaporation.

The previous study by Chen and Pereira [17] indi-

† Author to whom correspondence should be addressed.

## NOMENCLATURE

$C_p$	specific heat at constant pressure [J kg <sup>-1</sup> K <sup>-1</sup> ]	$T$	temperature [K]
$D_p$	droplet diameter [ $\mu\text{m}$ ]	$U$	axial gas velocity [m s <sup>-1</sup> ]
$H$	enthalpy of the gas phase [J kg <sup>-1</sup> ]	$V$	radial gas velocity [m s <sup>-1</sup> ]
$k$	turbulent kinetic energy [m <sup>2</sup> s <sup>-2</sup> ] or thermal conductivity [W m <sup>-1</sup> K <sup>-1</sup> ]	$x$	axial coordinate [m]
$L$	droplet latent heat of vaporization [J kg <sup>-1</sup> ]	$y$	radial coordinate [m].
$Le$	Lewis number, $Le = k_m/(\rho_m C_{pm} D_v)$	<b>Greek symbols</b>	
$m_p$	droplet mass, $m_p = \pi \rho_p D_p^3/6$ [kg]	$\varepsilon$	dissipation rate of turbulence [m <sup>2</sup> s <sup>-3</sup> ]
$\dot{N}$	droplet number flowrate [s <sup>-1</sup> ]	$\mu$	laminar dynamic viscosity [kg m <sup>-1</sup> s <sup>-1</sup> ]
$P$	pressure [N m <sup>-2</sup> ]	$\mu_t$	turbulent dynamic viscosity, $\mu_t = 0.09 \rho k^2/\varepsilon$ [kg m <sup>-1</sup> s <sup>-1</sup> ]
$Pr$	Prandtl number, $Pr = C_{pm} \mu_m/k_m$	$\rho$	density [kg m <sup>-3</sup> ].
$Sc$	Schmidt number, $Sc = \mu_m/(\rho_m D_v)$	<b>Subscripts</b>	
$S_m^p$	mass source from droplet phase [kg s <sup>-1</sup> ]	$i, j$	indices of coordinate component
$S_H^p$	enthalpy source from droplet phase [J s <sup>-1</sup> ]	$l$	liquid
$S_k^p$	turbulent energy source from droplet phase [kg m <sup>2</sup> s <sup>-3</sup> ]	$p$	droplet phase
$S_{U_i}^p$	momentum sources from droplet phase [kg m s <sup>-2</sup> ]	$t$	turbulent
$S_{\bar{u}_i \bar{u}_j}^p$	stress sources from droplet phase [kg m <sup>2</sup> s <sup>-3</sup> ]	$v$	fuel vapor or radial velocity component
$Sc_t$	turbulent model constant, $Sc_t = 0.7$	$m$	gas-film mixture.
$t$	time [s]	<b>Superscripts</b>	
		$\sim$	instantaneous
		$\cdot$	time derivative.

cates that the isotropic droplet-eddy encounter dispersion model of Gosman and Ioannides [18] fails to account for the effect of the anisotropy of gas turbulence on droplet dispersion for the present flow configuration whereas the time-correlated dispersion model of Zhou and Leschziner [19] can account for this anisotropic effect and gives more agreeable predictions with the measurements. Unfortunately, it is found that the mass-flux predictions tend to accumulate strongly near the centreline far downstream in both of these two droplet dispersion models. Therefore, another objective of the work is to improve the mass-flux predictions by devising a new approach for Lagrangian stochastic sampling. This new approach is also compared with another approach suggested by MacInnes and Bracco [20], which is associated with the time-correlated dispersion model of Zhou and Leschziner [19]. The efficiency of these two approaches to damp the mass-flux accumulation was assessed in terms of the experimental measurements. Besides, all the other numerical results were also discussed and appraised in accordance with the experimental measurements of Sommerfeld *et al.* [16].

## DESCRIBING EQUATIONS FOR THE GAS PHASE

The equations governing the continuous gas flow-field are modeled using the Reynolds-stress-transport (RST) model. For a steady, axisymmetric, two-dimen-

sional (2D) turbulent flow, application of the Reynolds time-averaging process to the Eulerian form of conservation equations for each dependent variable yields the governing equations for mass, momentum, enthalpy and vapor mass fraction as follows:

$$\frac{\partial \rho U_j}{\partial x_j} = S_m^p \quad (1)$$

$$\frac{\partial \rho U_i U_j}{\partial x_j} = -\frac{\partial P}{\partial x_i} + \frac{\partial}{\partial x_j} \left( \mu \frac{\partial U_i}{\partial x_j} - \rho \overline{u_i u_j} \right) + S_{U_i}^p \quad (2)$$

$$\frac{\partial \rho U_j H}{\partial x_j} = \frac{\partial}{\partial x_j} \left( \frac{\mu}{Pr} \frac{\partial H}{\partial x_j} - \rho \overline{u_j h} \right) + S_H^p \quad (3)$$

$$\frac{\partial \rho U_j F}{\partial x_j} = \frac{\partial}{\partial x_j} \left[ \frac{\mu}{Sc} \frac{\partial F}{\partial x_j} - \rho \overline{u_j f} \right] + S_m^p \quad (4)$$

where all the turbulent fluctuating correlations are modeled using the RST model, except that the mass fraction correlation is modeled using an isotropic eddy-viscosity diffusivity model, i.e.

$$-\rho \overline{u_i f} = \frac{\mu_t}{Sc_t} \frac{\partial F}{\partial x_i} \quad (5)$$

The Reynolds stresses can be expressed tensorially as

$$\frac{\partial}{\partial x_k} (\rho U_k \overline{u_i u_j}) = \frac{\partial}{\partial x_k} \left[ (\mu \delta_{mk} + \rho C_s \frac{k}{\varepsilon} \overline{u_k u_m}) \frac{\partial \overline{u_i u_j}}{\partial x_m} \right]$$

$$\begin{aligned}
& + P_{ij} + C'_1 \rho \frac{\varepsilon}{k} (\overline{u_i u_m} n_m \delta_{ij} - \frac{3}{2} \overline{u_i u_j} n_j) \\
& - \frac{3}{2} \overline{u_i u_j} n_j f_k - C_1 \rho \frac{\varepsilon}{k} (\overline{u_i u_j} - \frac{2}{3} k \delta_{ij}) - \frac{2}{3} \rho \varepsilon \delta_{ij} \\
& + C'_2 \frac{\varepsilon}{k} (\phi_{lm,2} n_l n_m \delta_{ij} - \frac{3}{2} \phi_{l,2} n_l n_j) \\
& - \frac{3}{2} \phi_{j,l,2} n_l n_j f_k - C_2 (P_{ij} - \frac{2}{3} G \delta_{ij}) + S_{\overline{u_i u_j}}^p
\end{aligned} \quad (6)$$

where the production  $G = P_{kk}/2$ ;  $n_i$  stands for the unit vector in the  $i$ -component normal to the wall; subscript  $k$  takes the same value as 1 but without summation;  $P_{ij}$  and  $f_k$  are given by

$$P_{ij} = - \left( \overline{\rho u_j u_k} \frac{\partial U_i}{\partial x_k} + \rho u_i u_k \frac{\partial U_j}{\partial x_k} \right) \quad (7)$$

$$f_k = \frac{k^{3/2}}{2.5 x_{kw} \varepsilon} \quad (8)$$

where  $x_{kw}$  is the normal distance from the wall. The heat-flux vector transport equations can be written as follows:

$$\begin{aligned}
\frac{\partial}{\partial x_j} (U_j \overline{u_i h}) & = -\rho \left( \overline{u_i u_j} \frac{\partial H}{\partial x_j} + \overline{u_j h} \frac{\partial U_i}{\partial x_j} \right) \\
& + \frac{\partial}{\partial x_j} \left[ \left( \frac{\mu}{Pr} + \rho C_h \frac{k}{\varepsilon} \overline{u_i u_k} \right) \frac{\partial \overline{u_i h}}{\partial x_k} \right] \\
& - C_{h1} \rho \frac{\varepsilon}{k} \overline{u_i h} + C_{h2} \rho \overline{u_j h} \frac{\partial U_i}{\partial x_j}. \quad (9)
\end{aligned}$$

Finally, the equation governing the dissipation rate of the turbulent kinetic energy is modeled by

$$\begin{aligned}
\frac{\partial}{\partial x_j} (\rho U_j \varepsilon) & = \frac{\partial}{\partial x_j} \left( \mu \frac{\partial \varepsilon}{\partial x_j} + C_{\varepsilon 2} \rho \frac{k}{\varepsilon} \overline{u_i u_j} \frac{\partial \varepsilon}{\partial x_i} \right) \\
& + (C_{\varepsilon 1} G - C_{\varepsilon 2} \rho \varepsilon) \frac{\varepsilon}{k} + C_{\varepsilon 3} S_k^p \frac{\varepsilon}{k}. \quad (10)
\end{aligned}$$

The RST model constants are given in Table 1. The determination of the droplet sources in the gas-phase equations is detailed elsewhere in Chen [21].

### DESCRIBING EQUATIONS FOR THE DROPLET PHASE

Having analysed the order of magnitude, Faeth [3] concluded that all forces, except the drag force, acting on the droplet will be negligible when the ratio of the gas to droplet density is very small. Under this

assumption, the equations of the motion for each of the droplet parcels can be written as

$$\frac{d\tilde{U}_{pi}}{dt} = \frac{\tilde{U}_i - \tilde{U}_{pi}}{\tau_p} + F_{pi} \quad (11)$$

where  $\tilde{U}_i = U_i + u_i$  is the instantaneous gas velocity, and  $F_{pi}$  are the external forces, i.e. gravity, centrifugal and Coriolis forces in the cylindrical coordinates. The relaxation time of droplets,  $\tau_p$ , is defined as

$$\tau_p = \frac{\rho_p D_p^2}{18 \mu_m f_p} \quad (12)$$

where the drag correction coefficient  $f_p$  depends on the relative Reynolds number between the gas and droplet phases, i.e.,

$$f_p = 1 + 0.15 Re_p^{0.687} \quad (0 < Re_p < 1000),$$

$$Re_p = \frac{\rho \sqrt{(\tilde{U}_{pi} - \tilde{U}_i)^2} D_p}{\mu_m}. \quad (13)$$

The droplet trajectories are computed by

$$\frac{dx_{pi}}{dt} = \tilde{U}_{pi}. \quad (14)$$

Note that in the above calculation the viscosity  $\mu_m$  is evaluated using the 1/3-rule for averaging of the gas-film condition. But the density is still based on the free stream value. This treatment is justified and recommended by Yuen and Chen [22] through their experiment, and is also numerically proved by Hubbard *et al.* [23].

### STOCHASTIC DROPLET DISPERSION MODELS

As is known, the main difficulty in Lagrangian computations is the unknown instantaneous gas field. The time-averaged Eulerian equations can only provide the gas mean properties. Therefore, the stochastic models have to be employed to account for the gas-phase turbulence on droplet dispersion. Currently, the most popular and simple dispersion model should be that due to Gosman and Ioannides [18]. This model is, however, in essence an isotropic dispersion model. It treats the droplet dispersion by employing the instantaneous gas velocity through the concept of droplet-eddy interactions. The droplets are assumed to interact with a sequence of randomly sampled turbulent eddies. The droplet-eddy interaction time is determined by minimizing two time scales: the eddy-life time and eddy-transit time. The fluctuating velocity is obtained by randomly sampling a Gaussian

Table 1. RST model constants

$C_s$	$C_1$	$C_2$	$C'_1$	$C'_2$	$C_{\varepsilon 1}$	$C_{\varepsilon 2}$	$C_{\varepsilon 3}$	$C_h$	$C_{h1}$	$C_{h2}$
0.22	1.8	0.6	0.5	0.3	1.45	1.90	1.10	0.3	3.2	0.5

PDF with a standard deviation of  $\sqrt{(2k/3)}$ . This model accounts for no temporal and directional correlations of velocity fluctuations, and can not take into account the anisotropic effect of gas turbulence on droplet dispersion. To overcome this model deficiency, Zhou and Leschziner [19] proposed a time-correlated model which accounts for temporal and directional correlations of velocity fluctuations between two successive time steps by

$$u_i(t) = \beta_{ij}u_j(t-\Delta t) + d_i \quad (15)$$

where  $\beta_{ij}$  is a coefficient matrix accounting for the effect from the previous time level and  $d_i$  accounts for the effect due to the randomness during the time interval  $\Delta t$ . The determination of these coefficients and some improvements can be found elsewhere in Zhou and Leschziner [18] as well as Chen and Pereira [17], respectively.

The comparative study [17] of these two dispersion models shows that the time-correlated dispersion model can adequately account for the anisotropy of turbulence, thus giving better prediction of droplet r.m.s. velocities than the isotropic dispersion model; however, the prediction of droplet mass fluxes tends to accumulate unrealistically near the centreline far downstream in both droplet dispersion models. Actually, this kind of phenomenon has already been observed by Adeniji-Fashola and Chen [24] in their Eulerian-Lagrangian computations. Therefore, it is necessary to develop an approach capable of eliminating this aphysical mass-flux accumulation. To this end, we modify the conventional SSF models to account for the anisotropic effect of gas turbulence on droplet dispersion as follows:

$$u_i = \sigma_i \xi_j \delta_{ij} \quad (16)$$

where  $\xi_j$  is a Gaussian random variable having zero mean and unity deviation,  $\sigma_i$  the standard deviation of fluctuating velocity, given presently by

$$\sigma_i = \sqrt{\langle u_i^2 \rangle}. \quad (17)$$

Instead of using  $\sqrt{(2k/3)}$  as done by Gosman and Ioannides [18], the normal stresses,  $u_i^2$ , are used in equation (17), which are obtained with the RST model predictions. To improve the mass-flux prediction, a new approach is developed in this work which modifies the way to sample the transverse component of the fluctuating velocity in equation (16). Rather than using the simple Gaussian variable for the transverse component, we use the following approach to obtain the random variable (details can be found in the Appendix)

$$\xi'_v = \xi'_v + \frac{\sigma_v}{y_p} \tau_p \alpha_p \quad (18)$$

where  $\xi'_v$  is the Gaussian variable having zero mean and unity deviation,  $\alpha_p$  a controlling parameter, being either zero or unity, to switch on or off this modification, depending on the local radial gas mean velocity, i.e.

$$\alpha_p = \frac{1}{2} \left( \frac{|V+0.015|}{V+0.015} + 1 \right) \quad (19)$$

where  $V$  is the radial mean velocity of the gas phase. The idea behind equation (19) is that the modification is switched off at  $V < -0.015 \text{ m s}^{-1}$ , which corresponds to the flow recirculating region. This is because droplets may physically accumulate in the recirculating region due to flow entrainment. Numerical experiments also prove the correctness of this reasoning. If we do not switch off the modification in this region, the droplets will be depleted from the centreline close to the inlet, which is against the experimental observation.

Using the time-correlated dispersion model, MacInnes and Bracco [20] proposed another method to overcome the mass-flux accumulation under the premise that the velocity fluctuation increment at time  $\Delta t$  should be compatible with the average fluctuating acceleration, i.e.

$$\overline{\Delta u_i} = \frac{\partial \overline{u_i}}{\partial x_j} \Delta t \quad (20)$$

which is added to the right-hand side of equation (15) as a drift correction.

## DROPLET EVAPORATION MODELS

In the spray considered here, the droplet evaporation, with an initial temperature of 313 K, occurs in a low temperature environment. The maximum inlet gas temperature is 373 K, while the droplet boiling temperature at atmospheric pressure is 355 K. The evaporation is mainly mass transfer controlled. Therefore, it is adequate to consider the droplet preheating process during its evaporation; see Sommerfeld *et al.* [16]. Berlemont *et al.* [25] reported that no substantial difference can be found between the results with the infinite-conduction model and the results with the conduction-limit model for their case studied. At present, two fashions of infinite-conduction evaporation model are considered for present spray evaporation, aiming at investigating the sensitivity of droplet properties to the two evaporation models.

### Model 1

The heat balance equation for the droplet is written as

$$m_p C_{pl} \frac{dT_p}{dt} = \pi D_p N u k_m (T - T_p) - \dot{m}_p L. \quad (21)$$

The classical  $d^2$ -law by Spalding [26] is used for mass evaporation rate, i.e.

$$\dot{m}_p = \pi D_p \rho_m D_v Sh \ln(1 + B_M) \quad (22)$$

where  $B_M$  is the Spalding mass transfer number,  $D_v$ , the binary diffusivity. The vapour mass fraction at the droplet surface is determined by the Clausius-Clapeyron's equilibrium vapour pressure equation;

see Chen and Pereira [27] for more details. To take into account the gas-phase convective effect on droplet evaporation, the following correlations are used to modify the Nusselt and Sherwood numbers:

$$\begin{aligned} Nu &= (2 + 0.55 Re_p^{1/2} Pr^{1/3})(1 + 1.232 Re_p^{-1} Pr^{-4/3})^{-1/2} \\ Sh &= (2 + 0.55 Re_p^{1/2} Sc^{1/3})(1 + 1.232 Re_p^{-1} Sc^{-4/3})^{-1/2} \end{aligned} \quad (23)$$

#### Model 2

Considering the blowing effect on droplet evaporation, Abramzon and Sirignano [28] suggested that the droplet surface temperature be computed by

$$m_p C_{pl} \frac{dT_p}{dt} = \dot{m}_p \left[ \frac{C_{pv}(T - T_p)}{B_T} - L \right] \quad (24)$$

where the Spalding heat transfer constant is given by

$$B_T = (1 + B_M)^\phi \quad \phi = \frac{C_{pv}}{C_{pm}} \frac{Sh^*}{Nu^*} \frac{1}{Le}. \quad (25)$$

The modified Nusselt and Sherwood numbers are given by

$$\begin{aligned} Nu^* &= 2 + \frac{Nu - 2}{F_T} \quad F_T = \frac{(1 + B_T)^{0.7}}{B_T} \ln(1 + B_T) \\ Sh^* &= 2 + \frac{Sh - 2}{F_M} \quad F_M = \frac{(1 + B_M)^{0.7}}{B_M} \ln(1 + B_M). \end{aligned} \quad (26)$$

The mass evaporation rate,  $\dot{m}_p$ , is determined similarly using equation (22) except that  $Sh$  is replaced by  $Sh^*$ . Note that  $B_T$  should be obtained iteratively with a given temperature. Details on finding  $B_T$  can be found in Abramzon and Sirignano [28].

#### COMPUTATION OF DROPLET PROPERTIES

Droplet properties are generally determined in terms of the number-averaged values, except mass flux and volume concentration which are obtained using the absolute number of droplets in the control volume considered. The general number-averaged property in a control volume ( $i, j$ ) can be determined by

$$\Phi_{p,ij} = \frac{\sum_{k=1}^M \Phi_{p,k} \dot{N}_k \Delta t_k}{\sum_{k=1}^M \dot{N}_k \Delta t_k} \quad (27)$$

where subscript  $k$  represents the  $k$ th droplet parcel crossing the control volume,  $\Delta V_{ij}$ ,  $M$  the total number of all droplet trajectories crossing the control volume. However, the droplet mass flux or volume concentration is computed differently. Taking the mass flux for example, we have

$$F_{p,ij} = \Delta V_{ij}^{-1} \sum_{k=1}^M \frac{\pi}{6} \rho_p D_p^3 \tilde{U}_{p,k} \dot{N}_k \Delta t_k. \quad (28)$$

Bearing these caveats in mind, we are going to explain why the accumulation phenomenon occurs only in the prediction of mass fluxes rather than in the other droplet properties.

#### NUMERICAL SOLUTION PROCEDURE

The finite-volume method is employed to solve the Eulerian equations together with a staggered mesh arrangement. The solution procedure for the gas phase follows the SIMPLE algorithm. The third-order discretization of the QUICK [29] algorithm was used for convection discretization. In solving the Reynolds-stress and heat flux equations, the apparent viscosities suggested by Huang and Leschziner [30] were used to obtain the explicitly diffusive terms in the momentum and enthalpy equations. The droplet-phase field is calculated by tracking the droplet parcels throughout the computational domain. The droplet equation of motion is presently solved in terms of cartesian coordinates to avoid the singularity that droplet radial position may approach zero in the application of the axisymmetric cylindrical coordinates. The droplet surface temperature and diameter are determined in an iterative way to enhance the strict conservation of mass and energy across the liquid interface. The droplet diameter change within an intergral time step,  $\Delta t$ , is determined by

$$D_p(t) = \sqrt{[D_p^2(t - \Delta t) - 4\lambda \Delta t / \rho_p]} \quad (29)$$

where

$$\lambda = \begin{cases} \rho_m D_v Sh \ln(1 + B_M) & \text{Model 1} \\ \rho_m D_v Sh^* \ln(1 + B_M) & \text{Model 2.} \end{cases} \quad (30)$$

The fully-implicit temporal discretization is used to compute the change of the droplet surface temperature under the assumption that gas temperature is constant within the integral time step, yielding

$$T_p(t) - T_p(t - \Delta t) = \frac{6\lambda \Delta t}{C_{pl} \rho_p \bar{D}_p^2} \{\Omega [T - T_p(t)] - L\} \quad (31)$$

where  $\Omega$  depends on the evaporation model, i.e.

$$\Omega = \begin{cases} \frac{Nu \cdot k_m}{\lambda} & \text{Model 1} \\ \frac{C_{pv}}{B_T} & \text{Model 2.} \end{cases} \quad (32)$$

The mean diameter used in equation (31) is determined by averaging the values between the two time steps, i.e.

$$\bar{D}_p^2 = \frac{1}{2} [D_p^2(t) + D_p^2(t - \Delta t)]. \quad (33)$$

Equation (31) can be solved efficiently using the Newton-Raphason iterative method, during which the droplet diameter can also be obtained. Note that the 1/3-rule averaging is used to compute all the variable

gas–film thermophysical properties in these equations; see Chen [21] for details. In addition, particular attention has to be paid to computing the droplet surface temperature due to the intrinsic “stiffness” in the droplet-temperature equation, as explained by Crowe [31]. This requires using small timesteps to advance the droplet ordinary-differential equations, especially when droplet diameters become very small due to spray evaporation.

### THE SPRAY CONFIGURATION

The experimental configuration for the hollow-cone spray used by Sommerfeld *et al.* [16] is shown in Fig. 1. The isopropyl-alcohol liquid was injected from the central nozzle with a diameter of 20 mm. A coflowing air stream was blown downwards through an annulus with an outer diameter of 64 mm. The detailed experimental measurements of radial profiles were performed radially at  $X = 3, 25, 50, 100, 200, 300$  and 400 mm. The first radial profile at  $X = 3$  mm was used as the initial conditions for the numerical computations. The remaining profiles were used as the validation of the numerical results. The first profile of measurements provides such detailed droplet properties as droplet sizes and their corresponding PDF distributions, mean and r.m.s. velocities for each of the droplet sizes, mass fluxes, and droplet mean diameters at each measured point. The geometry shown in Fig. 1 indicates that the test section had an inner diameter of 194 mm. The average temperatures of air and isopropyl-alcohol liquid at the inlet were 373 K and 313 K, respectively. The room temperature is about 303.4 K. The distribution of gas temperature along the wall was measured and will be used as the near-wall boundary condition for the enthalpy equation. The

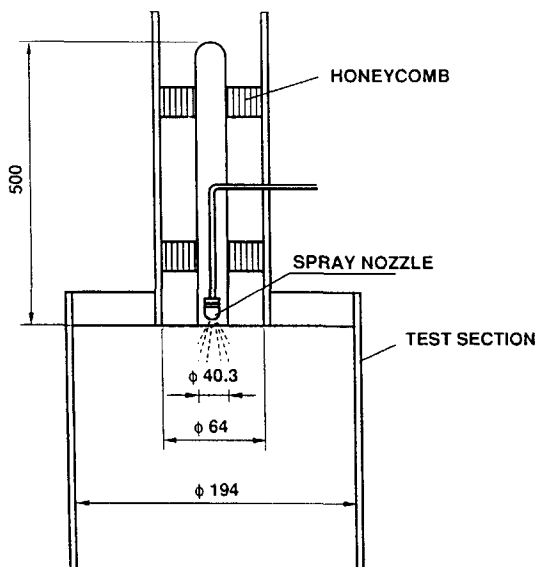


Fig. 1. Experimental flow configuration of Sommerfeld *et al.* (1993).

maximum air velocity at the inlet was  $18 \text{ m s}^{-1}$ . The inlet air mass flowrate was  $28.3 \text{ g s}^{-1}$ , and the inlet isopropyl-alcohol liquid mass flowrate was  $0.443 \text{ g s}^{-1}$ ; therefore, the spray was very dilute.

### RESULTS AND DISCUSSION

Experimental measurements indicate that the spray is approximately axisymmetric. To save computer CPU time and have more refined grids, only half of the flow domain was considered in the numerical calculations. The dimension of the computational domain was 1.3 m axially by 0.097 m radially. The following computations were performed using a grid of  $60 \times 53$  in the axial and radial directions, respectively, which was determined by numerical experiments. This grid distribution yields similar results to those obtained using  $85 \times 70$  control volumes. To well resolve the flow near the nozzle, refined grids were distributed near the recirculating region close to the inlet centreline. The following numerical runs, described in Table 2, have been performed for the present sensitivity study. Note that the number of trajectories here refers to the number of droplet parcels multiplied by the random walks. The selection of droplet parcels was based on the measured droplet PDF distributions at the inlet. The initial droplet-size distribution of the spray is selected according to the given experimental PDF to obtain an adequate number of discrete parcels, each of which represents a set of droplets having the same size and initial conditions.

In the following paragraphs, numerical results are compared and discussed according to the experimentally measured radial profiles at  $X = 25, 50, 100, 200, 300$  and 400 mm. Even though a lot of numerical results are available, only a few representative ones are described. The main droplet properties investigated below are the droplet axial mean velocity, Sauter mean diameters, mass fluxes, and fluctuating velocities.

Figures 2 and 3 show the results of Run 1 and Run 2 using two different numbers of droplet trajectories with an aim to study the effect of the number of droplet trajectories on the droplet properties. Figures 2(a)–(c) compare the measured and predicted radial profiles of the droplet axial mean velocity, Sauter mean diameters and mass fluxes, respectively. It is shown that the axial mean velocity in Fig. 2(a) is not sensitive to the number of trajectories, and that the droplet Sauter mean diameters and mass fluxes in Figs. 2(b) and (c) are only marginally sensitive to the number of trajectories.

The effect of the number of droplet trajectories on the droplet turbulent properties is shown in Figs. 3(a) and (b) for the axial and radial r.m.s. velocities, respectively. It is clearly evident that the droplet r.m.s. velocities downstream of  $X = 300$  mm are discernibly influenced by the number of trajectories at the inlet. This is due to the fact that far downstream droplet diameters become small due to spray evaporation. It is well known that small droplets, due to their small

Table 2. Description of numerical runs

Number of runs	Number of trajectories	Evaporation models	Drift correction approaches	Stochastic models
1	3500	Model 1	equation (18)	equation (16)
2	10 000	Model 1	equation (18)	equation (16)
3	40 000	Model 1	equation (18)	equation (16)
4	10 000	Model 1	None	equation (16)
5	10 000	Model 1	None	equation (15)
6	10 000	Model 1	equation (20)	equation (15)
7	10 000	Model 2	equation (18)	equation (16)

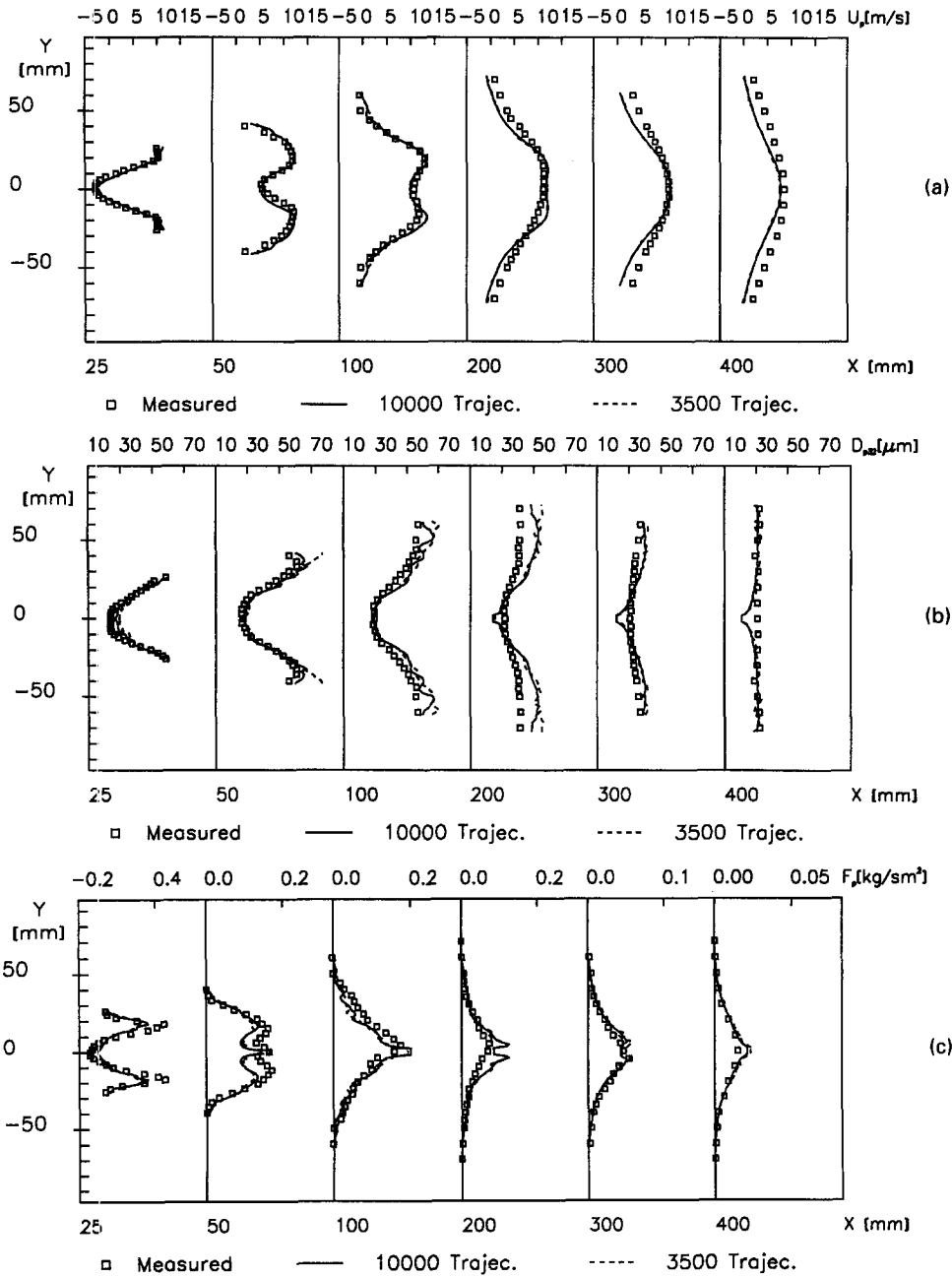


Fig. 2. Effect of the number of trajectories on droplet mean properties : (a) axial mean velocity; (b) Sauter mean diameter; and (c) mass flux.

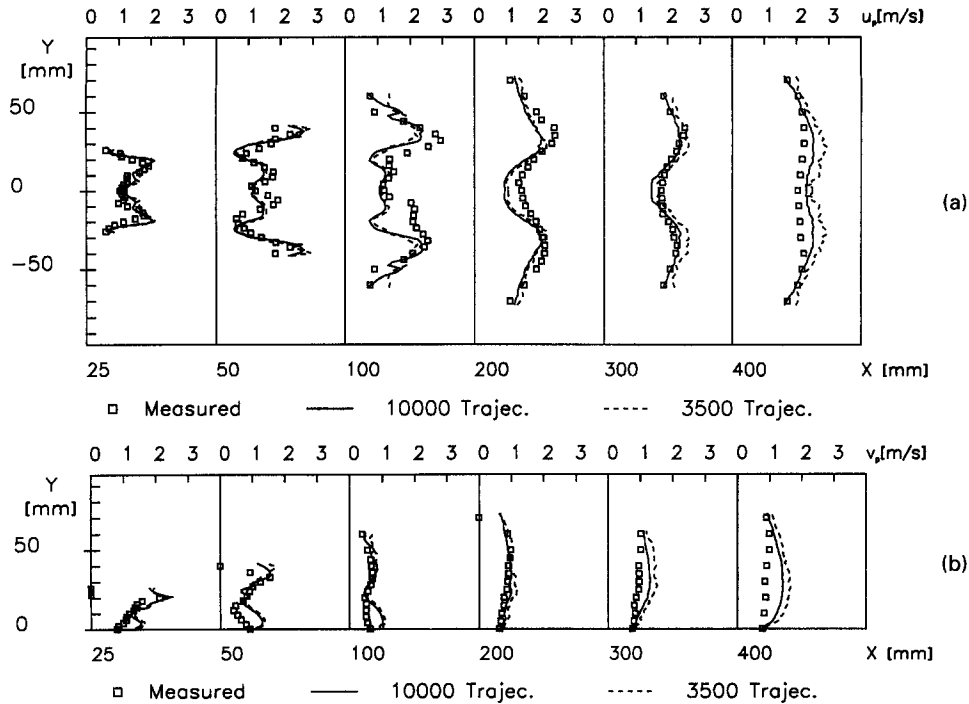


Fig. 3. Effect of the number of trajectories on droplet turbulent properties: (a) axial r.m.s. velocity and (b) radial r.m.s. velocity.

relaxation time constant, are very responsive to the change in gas turbulence; as a result, they are much influenced by the gas turbulence. Moreover, the total number of trajectories far downstream is relatively proportional to the total number of droplet trajectories at the inlet. Therefore, a larger number of droplet trajectories at the inlet results in a larger number of droplet trajectories downstream, thus yielding more reliable stochastic statistics far downstream. Consequently, the results obtained with a larger number of 10 000 trajectories are smoother and more agreeable with the measurements downstream. To see further whether the results with the 10 000 droplet trajectories are relatively independent of the number of trajectories, Figs. 4(a) and (b) compare, respectively, the droplet axial and radial r.m.s. velocities of Run 2 and Run 3 which are obtained with a total of 40 000 trajectories at the inlet. The other droplet properties are not shown here due to the very slight discrepancy between these two runs. The comparison demonstrates that almost no discrepancy can be distinguished; therefore, it can be deemed that the results with a total number of 10 000 trajectories at the inlet are invariant. As a consequence, all the following results are obtained with this number of trajectories.

The comparison of the mass-flux predictions with and without drift correction is shown in Figs. 5(a) and (b) in association with two droplet dispersion models. Figure 5(a) examines the effect of the new drift correction approach on the mass-flux predictions (Run 2

and Run 4) associated with a modified dispersion model. It clearly indicates that the mass-flux predictions tend to accumulate strongly downstream of  $X = 200$  mm (dashed line), whereas with the new drift correction of equation (18) the mass-flux prediction is substantially improved. Figure 5(b) examines the effect of the drift correction method due to MacInnes and Bracco [20] on the mass-flux predictions (Run 5 and Run 6). This drift correction method is associated with the time-correlated dispersion model of Zhou and Leschziner [19], which has been studied by Chen and Pereira [17] in comparison with the isotropic dispersion model of Gosman and Ioannides [18]. It can be seen that the incorporation of the drift correction term of equation (20) does improve the mass-flux predictions downstream of  $X = 300$ ; however, the accumulation of mass fluxes downstream is in essence still present. Therefore, the drift correction approach suggested by MacInnes and Bracco [20] does not work well for the evaporating spray investigated here, as far as the damping of mass-flux accumulation is concerned. To see further the improvement obtained with the present modified dispersion model, Fig. 5(c) compares the two mass-flux predictions obtained with the standard dispersion model of Gosman and Ioannides and with the modified SSF model. It is clearly evident that the present modified model substantially ameliorates these mass-flux predictions. It may be puzzling that the mass fluxes are strongly over-predicted far downstream whereas the other droplet

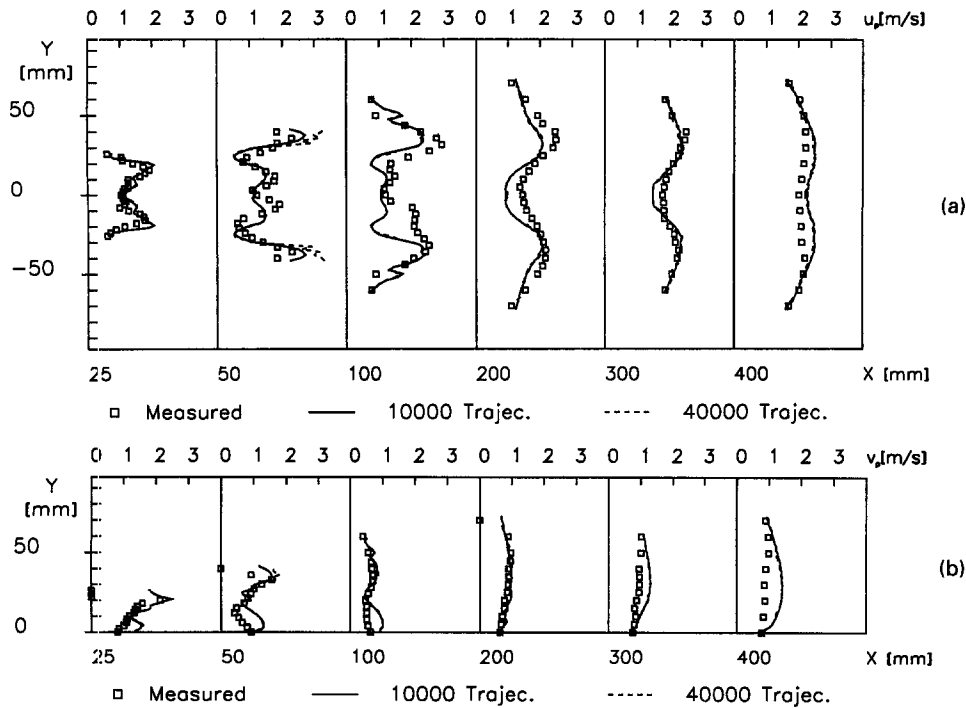


Fig. 4. Sensitivity of the droplet r.m.s. velocities to the number of trajectories: (a) axial r.m.s. velocity and (b) radial r.m.s. velocity.

properties can be satisfactorily predicted. The answer to this question is quite simple, if we examine the way to compute the droplet mass flux by equation (27) and the other properties by equation (28). The substantial difference between these two computations lies in the fact that the absolute number of droplets is used for the mass-flux calculation while the number-weighted averaging is used for the calculation of the other properties. Therefore, the droplet accumulation near the centreline results in only an overprediction of mass fluxes, but has no effect on the other number-weighted droplet properties.

Figures 6(a)–(c) compare the droplet fluctuating properties obtained with the present modified model and the standard model of Gosman and Ioannides. It can be seen that the modified model better predicts these droplet fluctuating properties, especially the droplet r.m.s. velocities, as compared to the standard Gosman and Ioannides model due to the account of anisotropy of turbulence in the modified model.

Figures 7(a)–(c) compare the results of Run 2 and Run 7 with the two fashions of infinite-conduction model. Figure 7(a) shows that the droplet axial mean velocity is not sensitive to the evaporation model whereas Fig. 7(b) shows that the droplet Sauter mean diameters are influenced by the evaporation models, especially downstream of  $X = 200$  mm. Figure 7(c) clearly demonstrates that the mass fluxes are sensitive

to the evaporation models. The results with evaporation model 2 accounting for the blowing effect slightly underpredict the Sauter mean diameters and mass fluxes in contrast to evaporation model 1. The two evaporation models behave in an opposite way in the prediction of mass fluxes between  $X = 200$  and  $300$  mm; see Fig. 7(c). The prediction of the Sauter mean diameters in Fig. 7(b) indicates that the evaporation model of Abramzon and Sirignano [28] is slightly better than evaporation model 1.

The effect of the two evaporation models on droplet turbulent properties is examined in Figs. 8(a) and (b) for the axial and radial r.m.s. velocities, respectively. It is evident that the two infinite-conduction evaporation models with and without the blowing effect have negligible influence on the droplet r.m.s. velocities. Finally, Fig. 9 shows the effect of the evaporation models on the droplet mass flowrate, which has been normalized by the value at the inlet. The mass flowrate  $\dot{M}$  is obtained by integrating the droplet mass flux over the cross-sectional area. It can be seen that the predictions with the two evaporation models agree satisfactorily with the measurements, especially far downstream. The discrepancy between the two models is small upstream of  $X = 25$  mm and downstream of  $X = 400$  mm, while relatively large discrepancy exists in between. This is consistent with the conclusion drawn by Aggarwal and Chitre [14], who found that

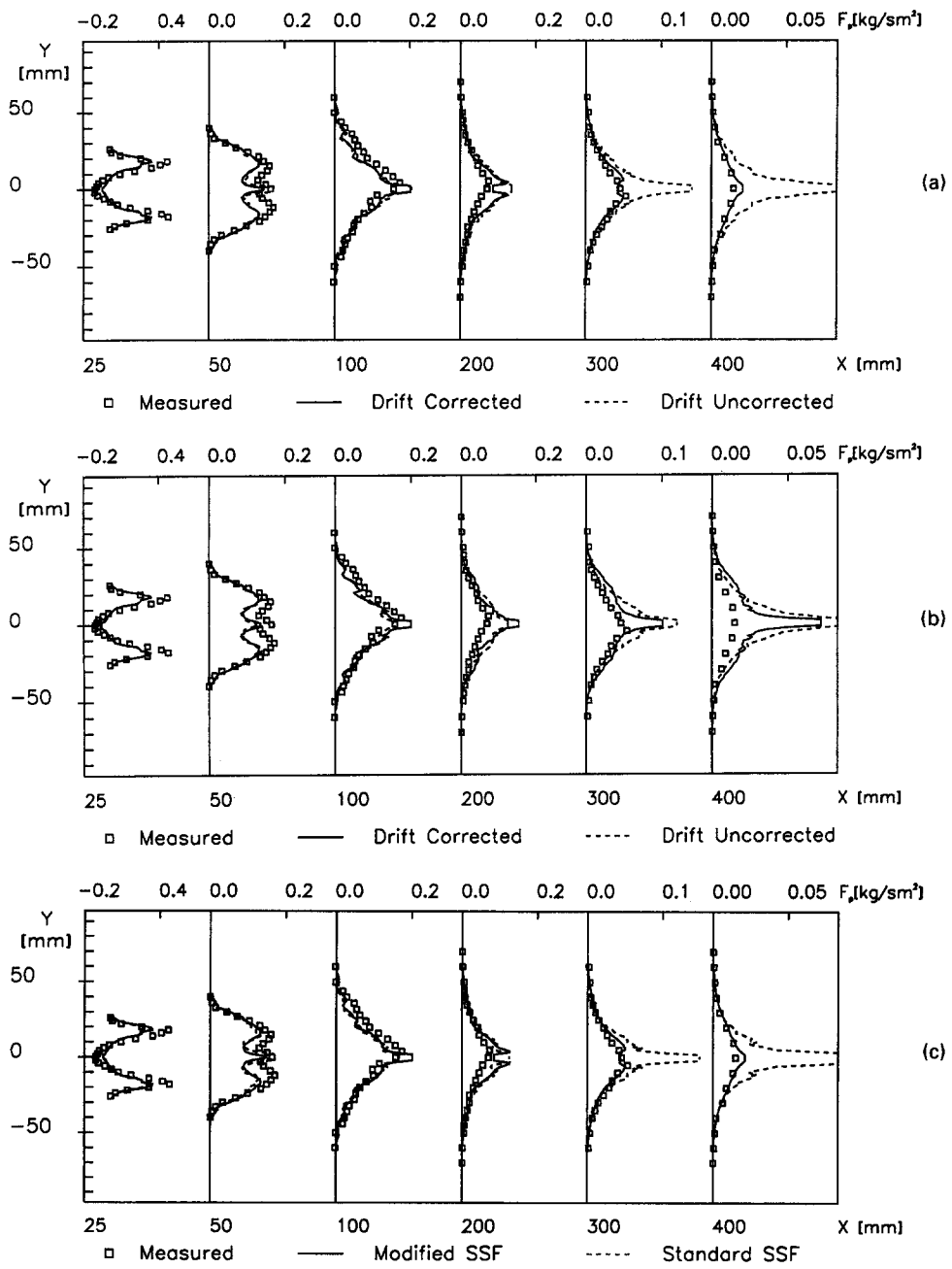


Fig. 5. Effect of the drift correction approaches on mass-flux predictions: (a) present new method with the modified SSF model; (b) method of MacInnes and Bracco with the time-correlated SSF model; and (c) modified model vs standard model.

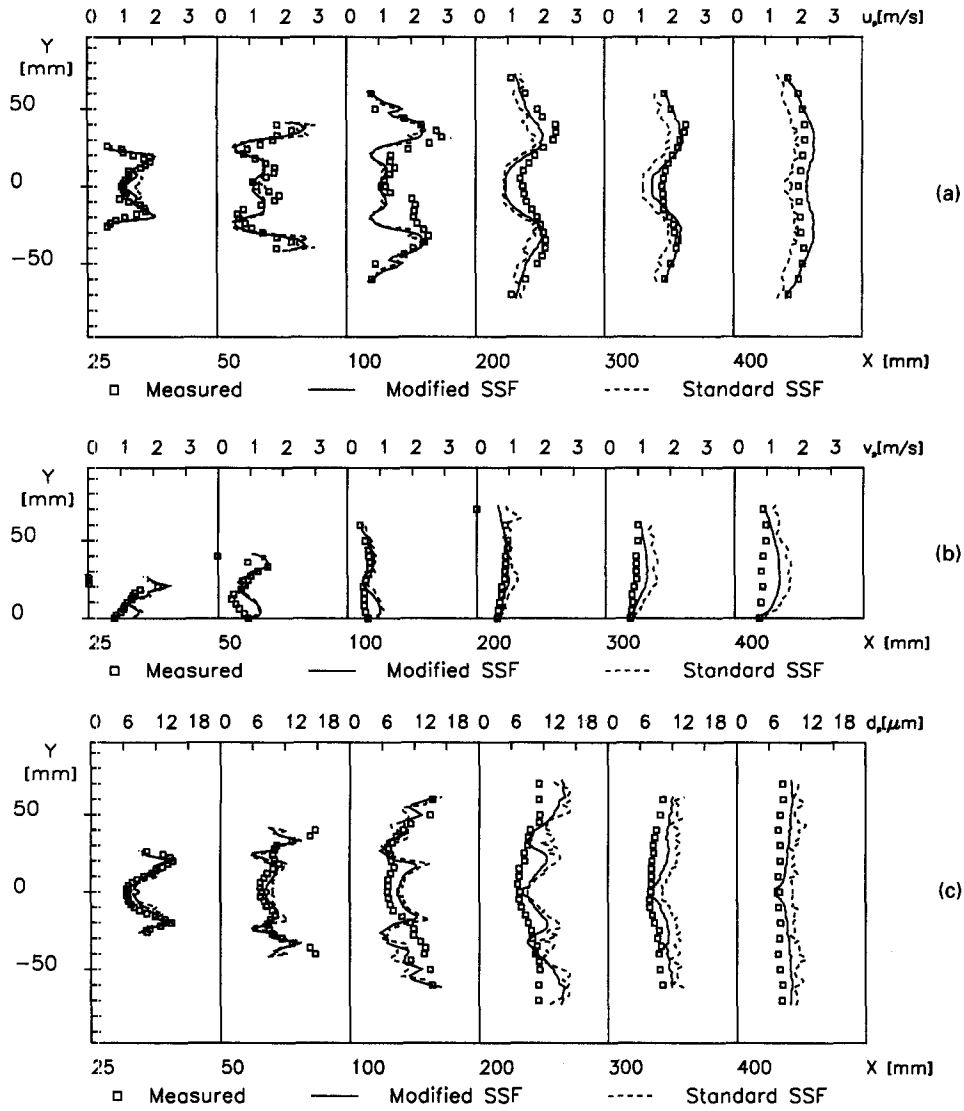


Fig. 6. Droplet fluctuating properties obtained with standard and modified models : (a) axial r.m.s. velocity ; (b) radial r.m.s. velocity ; and (c) droplet r.m.s. diameter.

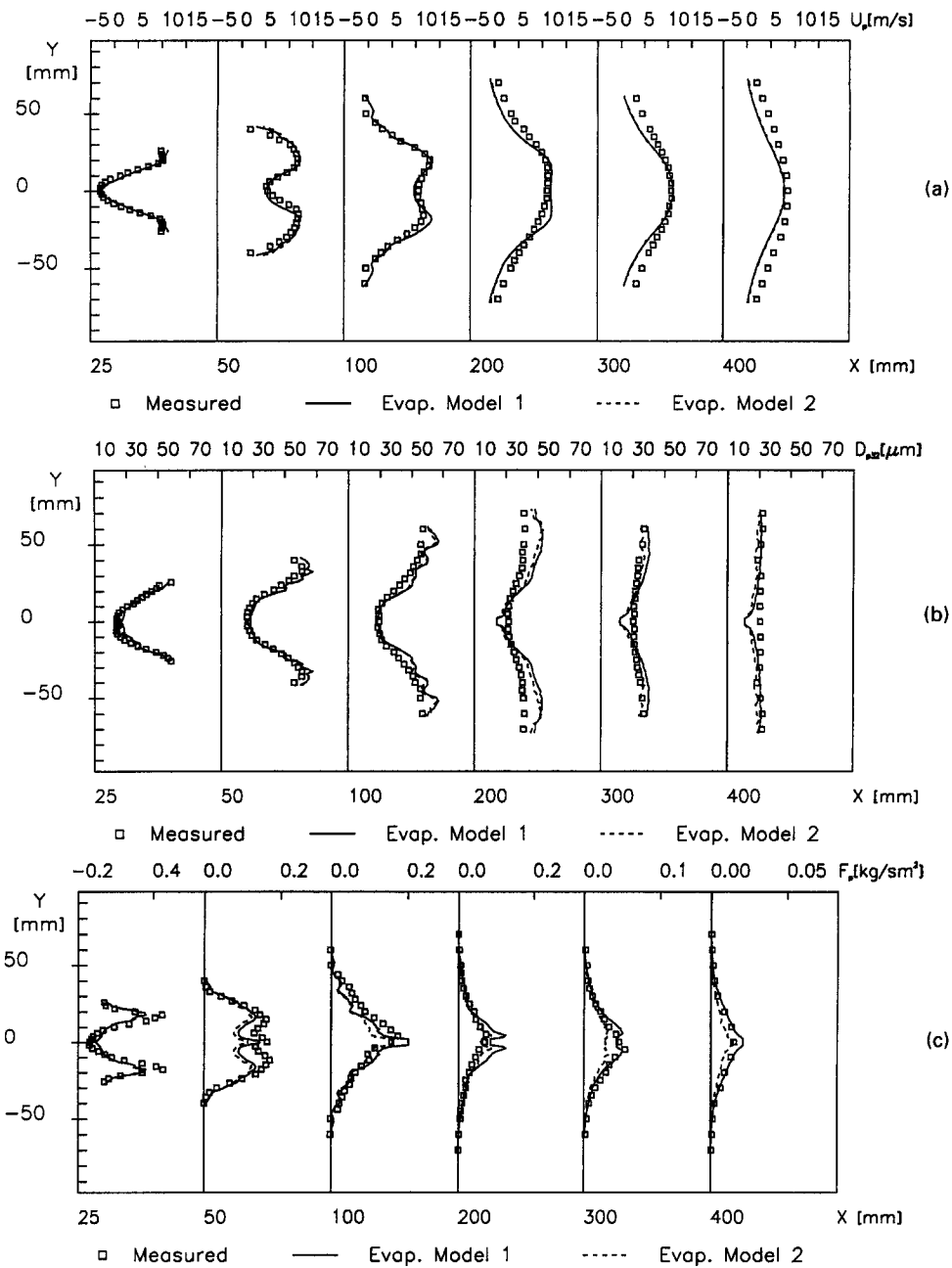


Fig. 7. Effect of the evaporation models on droplet mean properties: (a) axial mean velocity; (b) Sauter mean diameter; and (c) mass flux.

the vaporization models have relatively small effect on long time evaporation.

### CONCLUSIONS

A sensitivity study of droplet properties to various factors in the modeling of dilute evaporating sprays was conducted using the Eulerian-Lagrangian SSF models with the well-specified experimental measurements. The Eulerian formulation of the gas-phase flowfield was based on the second-order momentum turbulence closure with a high-order QUICK algo-

rithm used for convection discretization. The relatively reliable prediction of gas-phase normal stresses with the RST model makes it possible to successfully modify the conventional SSF models, where the droplet-encountered eddy turbulent properties are only based on the local turbulent kinetic energy, to account for the anisotropic effect of gas turbulence on droplet dispersion. Moreover, several problems associated with the modeling of dilute evaporating sprays have also been addressed in this work with particular emphasis attached to the sensitivity study of droplet properties. An overall satisfactory agreement has been

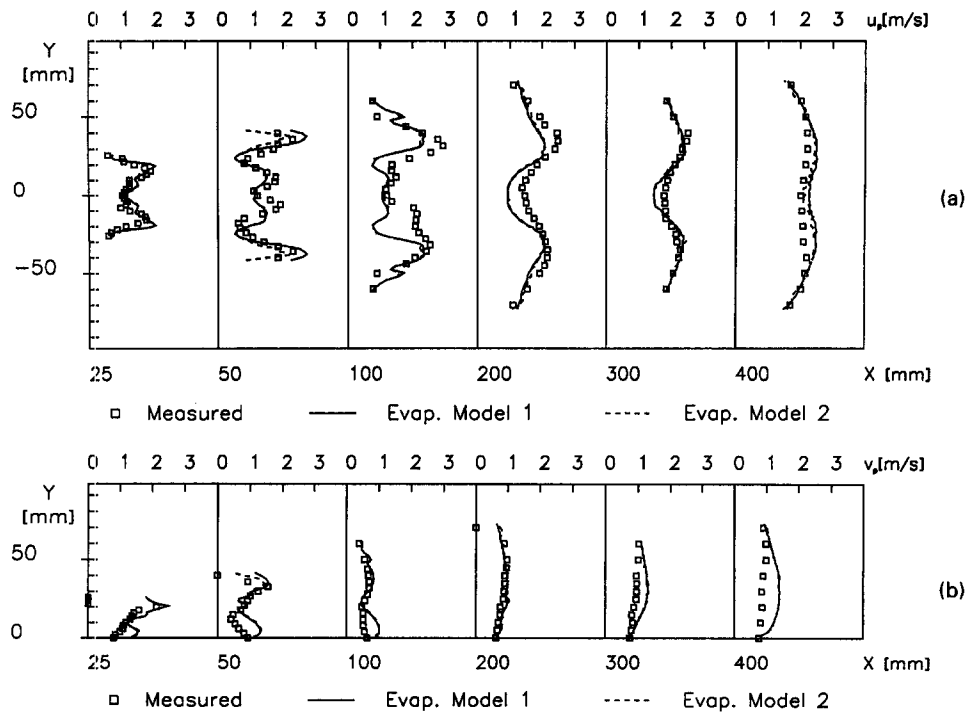


Fig. 8. Effect of the evaporation models on droplet turbulent properties: (a) axial r.m.s. velocity and (b) radial r.m.s. velocity.

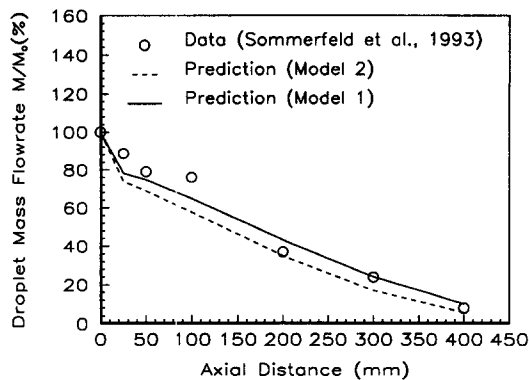


Fig. 9. Effect of the evaporation models on droplet mass flowrate.

achieved between the numerical predictions and the experimental measurements, showing that the Eulerian-Lagrangian model can be reliably used for the modeling of dilute evaporating sprays. The following conclusions can be drawn from the present sensitivity study:

(1) Droplet r.m.s. velocities far downstream are very sensitive to the number of droplet trajectories, and a total number of  $10^4$  droplet trajectories at the inlet should be considered.

(2) Droplet mean diameters were not much sensitive to the evaporation models selected; however, it was found that the predicted Sauter mean diameters using the evaporation model accounting for the blow-

ing effect are in better agreement with the measurements.

(3) A drift correction is required in axisymmetric flow configurations to avoid the artificial accumulation in mass-flux predictions at the centreline, and the present proposed approach can substantially improve the mass-flux prediction.

(4) Droplet mass fluxes are particularly sensitive to the evaporation models; the evaporation model with blowing effect tends to slightly underpredict the mass fluxes downstream whereas the evaporation model without blowing effect tends to overpredict the mass fluxes downstream.

*Acknowledgement*—This work was supported by the Commission of the European Communities (DGXII) under the project No. JOULE-CT91-0067 (TSTS).

## REFERENCES

1. N. A. Chigier, The atomization and burning of liquid fuel sprays, *Prog. Energy Combust. Sci.* **2**, 97–114 (1976).
2. C. K. Law, Recent advances in droplet vaporization and combustion, *Prog. Energy Combust. Sci.* **8**, 171–201 (1982).
3. G. M. Faeth, Evaporation and combustion of sprays, *Prog. Energy Combust. Sci.* **9**, 1–76 (1983).
4. C. T. Crowe, Review—numerical methods for dilute gas-particle flows, *J. Fluids Engng* **104**, 297–303 (1982).
5. W. A. Sirignano, The formulation of spray combustion models: resolution compared to droplet spacing, *J. Heat Transfer* **108**, 633–639 (1978).
6. W. A. Sirignano, Fluid dynamics of sprays—1992 Freeman scholar lecture, *J. Fluids Engng* **115**, 345–378 (1993).
7. J.-S. Shuen, A. S. P. Solomon, Q.-F. Zhang and G. M.

- Faeth, Structure of particle-laden jets: measurements and predictions, *AIAA J.* **23**, 396–404 (1985).
8. X.-Q. Chen and J. C. F. Pereira, Numerical prediction of evaporating and nonevaporating sprays under non-reactive conditions, *Atomization Sprays* **2**, 427–443 (1992).
  9. G. J. Sturgess, S. A. Syed and K. R. McManus, Calculation of a hollow-cone liquid spray in uniform airstream, *J. Propul. Power* **1**, 360–369 (1985).
  10. D. L. Bulzan, Y. Levy, S. K. Aggarwal and S. Chitre, Measurements and predictions of a liquid spray from an air-assist nozzle, *Atomization Sprays* **2**, 445–462 (1992).
  11. K.-C. Chang, M.-R. Wang, W.-J. Wu and C.-H. Hong, Experimental and theoretical study on hollow-cone spray, *J. Propul. Power* **9**, 28–34 (1993).
  12. A. S. P. Solomon, J.-S. Shuen, Q.-F. Zhang and G. M. Faeth, Structure of nonevaporating sprays—I. Initial conditions and mean properties, *AIAA J.* **23**, 1548–1555 (1985).
  13. A. S. P. Solomon, J.-S. Shuen, Q.-F. Zhang and G. M. Faeth, Structure of nonevaporating sprays—II. Drop and turbulence properties, *AIAA J.* **23**, 1724–1730 (1985).
  14. S. K. Aggarwal and S. Chitre, Computation of turbulent evaporating sprays, *J. Propul. Power* **7**, 213–220 (1991).
  15. A. S. P. Solomon, J.-S. Shuen, Q.-F. Zhang and G. M. Faeth, Measurements and predictions of the structure of evaporating sprays, *J. Heat Transfer* **107**, 679–686 (1985).
  16. M. Sommerfeld, H.-H. Qiu, M. Ruger, G. Kohnen and D. Muler, Spray evaporation in turbulent flow, *Proceedings of the 2nd Symposium on Engineering Turbulence Modeling and Measurements*, Florence, Italy, 31 May–1 June, pp. 935–945 (1993).
  17. X.-Q. Chen and J. C. F. Pereira, Prediction of evaporating spray in anisotropically turbulent gas flow, *Numer. Heat Transfer* **27**, 143–162 (1995).
  18. A. D. Gosman and E. Ioannides, Aspects of computer simulation of liquid-fuelled combustors, *AIAA paper* 81-0323 (1981).
  19. Q. Zhou and M. A. Leschziner, A time-correlated stochastic model for particle dispersion in anisotropic turbulence, *Proceedings of the 8th Turbulent Shear Flows Symposium*, Munich, September (1991).
  20. J. M. MacInnes and F. V. Bracco, Stochastic particle dispersion modeling and the tracer-particle limit, *Phys. Fluids A*, **4**, 2809–2824 (1992).
  21. X.-Q. Chen, Numerical simulation of steady and unsteady two-phase spray flows, Ph.D. Thesis, Instituto Superior Técnico, Technical University of Lisbon, Portugal (1994).
  22. M. C. Yuen and L. W. Chen, On drag of evaporating liquid droplets, *Combust. Sci. Technol.* **14**, 147–154 (1976).
  23. G. L. Hubbard, V. E. Denny and A. F. Mills, Droplet evaporation: effects of transients and variable properties, *Int. J. Heat Mass Transfer* **18**, 1003–1008 (1975).
  24. A. Adeniji-Fashola and C. P. Chen, Modeling of confined turbulent fluid-particle flows using Eulerian and Lagrangian schemes, *Int. J. Heat Mass Transfer* **33**, 691–701 (1990).
  25. A. Berlemont, M.-S. Grancher and G. Gouesbet, On the Lagrangian simulation of turbulence on droplet evaporation, *Int. J. Heat Mass Transfer* **34**, 2805–2812 (1991).
  26. D. B. Spalding, The combustion of liquid fuels, *Proceedings of 4th International Symposium on Combustion*, The Combustion Institute, Pittsburgh, PA., pp. 847–864 (1953).
  27. X.-Q. Chen and J. C. F. Pereira, On the influence of gas temperature on spray evaporation, *Proceedings of the International Symposium on Turbulence, Heat and Mass Transfer*, 9–12 August, Lisbon, Portugal, Vol. 1, pp. 10.2.1–10.2.7 (1994).
  28. B. Abramzon and W. A. Sirignano, Droplet vaporization model for spray combustion calculations, *Int. J. Heat Mass Transfer* **32**, 1605–1618 (1989).
  29. B. P. Leonard, A stable and accurate convective modeling procedure based on quadratic upwind interpolation, *Comput. Methods Appl. Mech. Engng* **19**, 59–58 (1979).
  30. P. G. Huang and M. A. Leschziner, Stabilization of recirculating-flow computations performed with second moment closures and third order discretization, *Proceedings of the 5th Symposium on Turbulent Shear Flows*, Cornell University, pp. 20.7–20.12 (1985).
  31. C. T. Crowe, Modeling spray-air contact in spray drying system, *Advances in Drying* (Edited by A. S. Mujumdar), Vol. 1, pp. 63–69. Hemisphere, New York (1980).

## APPENDIX A

In the axisymmetric cylindrical coordinates, the radial-momentum equation of a droplet parcel can be written as

$$\frac{d\tilde{V}_p}{dt} = \frac{\tilde{V} - \tilde{V}_p}{\tau_p} + \frac{\tilde{W}_p^2}{y_p} \quad (\text{A1})$$

where the second term on the r.h.s. denotes the centrifugal force, and is usually important only when the droplet is moving close to the symmetric axis for axisymmetric flows. Moreover, the mean gas tangential velocity is zero in axisymmetric flows. We may assume that  $\tilde{W}_p^2 \approx \sigma_w^2$ , with  $\sigma_w$  being the standard deviation of the gas tangential fluctuating velocity. Note that the radial gas instantaneous velocity is given by

$$\tilde{V} = V + \xi'_v \sigma_v \quad (\text{A2})$$

where  $\xi'_v$  is a Gaussian random variable. Incorporating these into equation (A1), we have

$$\frac{d\tilde{V}_p}{dt} = \frac{\left( V + \xi'_v \sigma_v + \frac{\sigma_w^2}{y_p} \tau_p \right) - \tilde{V}_p}{\tau_p} \quad (\text{A3})$$

Taking  $\xi'_v \sigma_v + \frac{\sigma_w^2}{y_p} \tau_p$  as an apparent radial gas fluctuating velocity,  $v$ , we can write

$$v = \xi'_v \sigma_v + \frac{\sigma_w^2}{y_p} \tau_p \quad (\text{A4})$$

If we further assume that  $\sigma_v = \sigma_w$ , then we finally obtain

$$v = \left( \xi'_v + \frac{\sigma_v}{y_p} \tau_p \right) \sigma_v = \xi_v \sigma_v \quad (\text{A5})$$

To correct the errors arising from the above assumptions used to derive equation (A5), another parameter,  $\alpha_p$ , has been used in equation (18), and is determined depending on the flow configuration.